ecules and salts (*19*) to organic macromolecules (*10*, *20*) on a variety of substrates. In addition, on both gold and silicon oxide, the transport rate of the DNA can be tailored with careful humidity control. It is thus possible to vary feature size over a large dynamic range on a reasonable time scale. For example, on gold, the diameter of a spot created by holding the AFM tip for 10 s changes from 50 to 300 nm with a relative humidity change of 15% (Fig. 3C). This humidity dependence points to a mechanism for transport of DNA from an AFM tip to a surface, which is dependent on the water meniscus between the tip and substrate (*21*).

To demonstrate multi-DNA ink capabilities, we have used DPN to prepare a two-component DNA array on an oxidized silicon substrate and verified its sequence-specific activity by hybridization with complementary fluorophore-labeled probes (Fig. 4A). To further verify the chemical integrity of the patterns, the same chip was treated with DI water to remove the fluorophore-labeled DNA and then exposed to a solution containing a mixture of 5- and 13-nm–diameter gold nanoparticles. The large and small particles were modified with DNA complementary to the first and second patterns, respectively. The particles selectively assembled on the correct patterns (Fig. 4B) under appropriate hybridization conditions. This experiment not only shows how one could potentially use nanoparticles as diagnostic probes in AFM-based screening procedures but also shows how one can use nanostructures fabricated by the direct-write DPN approach to control the assembly of nanoparticle-based architectures.

In view of the rapid proliferation of bioconjugated nanoparticle labels and building blocks (*22*–*24*), the method described here should allow the DPN- and DNA-templated assembly of a wide variety of metallic, semiconducting, magnetic, and insulating nanostructures, on both metallic and insulating substrates. These structures can in turn be used to address issues in molecular electronics, photonics, high-density information storage, and biosensing (*5*, *25*). The method also suggests new routes for investigating the fundamental limits of microarray miniaturization. With the resolution demonstrated here, arrays with ~100,000 oligonucleotide spots could be generated in an area the size of a typical AFM scanner (100 μm by 100 μm) on time scales comparable with those of conventional robotic spotting methods, thereby making possible the investigation of scanned probe methods of nano- and microarray fabrication and readout.

References and Notes

1. R. D. Piner, J. Zhu, F. Xu, S. Hong, C. A. Mirkin, *Science* **283**, 661 (1999).
2. S. Hong, J. Zhu, C. A. Mirkin, *Science* **286**, 523 (1999).
3. S. Hong, C. A. Mirkin, *Science* **288**, 1808 (2000).
4. J. J. Storhoff, C. A. Mirkin, *Chem. Rev.* **99**, 1849 (1999).
5. C. M. Niemeyer, *Angew. Chem. Int. Ed.* **40**, 4128 (2001).
6. L. M. Demers, S.-J. Park, T. A. Taton, Z. Li, C. A. Mirkin, *Angew. Chem. Int. Ed.* **40**, 3071 (2001).
7. P. V. Schwartz, *Langmuir* **17**, 5971 (2001).
8. K. B. Lee, S.-J. Park, C. A. Mirkin, J. C. Smith, M. Mrksich, *Science* **295**, 1702 (2002).
9. A. Ivanisevic, C. A. Mirkin, *J. Am. Chem. Soc.* **123**, 7887 (2001).
10. A. Noy *et al.*, *Nano Letters* **2**, 109 (2002).
11. C. A. Mirkin, *Mater. Res. Soc. Bull.* **25**, 43 (2000).
12. We have also successfully used cantilevers coated with an evaporated layer of Au and a self-assembled monolayer of cysteamine.
13. T. M. Herne, M. J. Tarlov, *J. Am. Chem. Soc.* **119**, 8916 (1997).
14. R. Levicky, T. M. Herne, M. J. Tarlov, S. K. Satija, *J. Am. Chem. Soc.* **120**, 9787 (1998).
15. D. G. Kurth, T. Bein, *Langmuir* **9**, 2965 (1993).
16. M. Kenney, S. Ray, T. C. Boles, *Biotechniques* **25**, 516 (1998).
17. J. Jang, S. Hong, G. C. Schatz, M. A. Ratner, *J. Chem. Phys.* **115**, 2721 (2001).
18. D. A. Weinberger, S. Hong, C. A. Mirkin, B. W. Wessels, T. B. Higgins, *Adv. Mater.* **12**, 1600 (2000).
19. B. W. Maynor, Y. Li, J. Liu, *Langmuir* **17**, 2575 (2001).
20. D. L. Wilson *et al.*, *Proc. Natl. Acad. Sci. U.S.A.* **98**, 13660 (2001).
21. R. P. Piner, S. Hong, C. A. Mirkin, *Langmuir* **15**, 5457 (1999).
22. M. Bruchez, M. Moronne, P. Gin, S. Weiss, A. P. Alivisatos, *Science* **281**, 2013 (1998).
23. S. R. Nicewarner-Pena *et al.*, *Science* **294**, 137 (2001).
24. Y. Cui, Q. Q. Wei, H. K. Park, C. M. Lieber, *Science* **293**, 1289 (2001).
25. C. A. Mirkin, *Inorg. Chem.* **39**, 2258 (2000).

26. C.A.M. acknowledges the Air Force Office of Scientific Research, the Defense Advanced Research Projects Agency, and the NSF for support of this research. L.M.D. is grateful to the Natural Sciences and Engineering Research Council of Canada for a graduate fellowship, and D.S.G. thanks the NIH (1 F32 HG02463) and DuPont for postdoctoral support.

Supporting Online Material

www.sciencemag.org/cgi/content/full/296/5574/1836/DC1

Materials and Methods

Figs S1 and S2

4 March 2002; accepted 22 April 2002

Probing High-Barrier Pathways of Surface Reactions by Scanning Tunneling Microscopy

M. Dürr,[1,2]* A. Biedermann,[1,3] Z. Hu,[1] U. Höfer,[2] T. F. Heinz[1]

The ability of scanning tunneling microscopy to probe the pathways of thermally activated high-barrier surface processes is frequently limited by competing low-barrier processes that can confuse measurement of the true initial and final configuration. We introduce an approach to circumvent this difficulty by driving the surface process with nanosecond laser heating. The method is applied to determine the pathway of recombinative desorption in the H/Si(001) system. The observed configuration of dangling bonds after laser heating reveals that the desorbed hydrogen molecules are not formed on single dimers, but rather from neighboring silicon dimers via an interdimer reaction pathway.

In recent years, scanning tunneling microscopy (STM) has become an important tool for elucidating the rates and pathways of dynamical processes at surfaces. In particular, the development of STM instrumentation capable of operating at variable temperature has enabled researchers to follow dynamical processes with atomically defined initial and final states. In this approach, the sample is held at a temperature where the process of interest occurs on a time scale comparable to that for STM data acquisition, typically a fraction of a second, and changes are recorded in real time. This approach has been remarkably effective in examining surface diffusion and other processes with low activation energy (*1*–*4*). A characteristic of surfaces, however, is the existence of competing reaction pathways. Many important processes, such as those leading to new species through surface reactions, have high activation energies. They generally proceed in the presence of rapid, low-barrier processes, thus confounding their observation by STM techniques.

Two of the most elementary surface processes, diffusion and desorption of adsorbates, are representative of this predicament, because the activation energy of the latter always exceeds that of the former. The situation is illustrated schematically in Fig. 1 for the system of H/Si(001) discussed below. The surface diffusion rate for adsorbed hydrogen can be described by an Arrhenius expression with an activation energy considerably less than that for the recombinative desorption process by which the adsorbed hydrogen atoms leave the surface. Thus, at temperatures where STM techniques can follow the motion of individual hydrogen

[1]Departments of Physics and Electrical Engineering, Columbia University, New York, NY 10027, USA. [2]Fachbereich Physik und Zentrum für Materialwissenschaften, Philipps-Universität Marburg, D-35032 Marburg, Germany. [3]Institut für Allgemeine Physik, Vienna University of Technology, A-1040 Vienna, Austria.

*To whom correspondence should be addressed. E-mail: duerr@physik.uni-marburg.de

adatoms, no desorption occurs. On the other hand, at temperatures at which desorption occurs, surface diffusion is so rapid that atomic positions cannot be captured by STM and no information about atomic pathways can be obtained. Moreover, examination of the surface after a conventional heating cycle that induces desorption will show a resulting configuration that reflects the equilibrium arrangement of the surface. The initial configuration produced immediately after desorption is destroyed by surface diffusion.

We introduce the use of single-shot laser-induced thermal desorption in combination with STM as an experimental approach to circumvent the difficulty of observing atomically defined pathways for such high-barrier processes. To achieve this goal, we need to reach elevated surface temperatures at which the processes with higher activation energy can compete with—or even outrun—processes with lower barriers. This change in relative rates is furthered by the compensation effect, which describes the frequently observed propensity of processes with high activation energy to be accompanied by high preexponential factors (*5*). However, to make use of this change in relative rates, it is necessary not only to reach high temperatures but to do so within a very brief period of time. This can be achieved with pulsed laser radiation, a method capable of providing heating rates in excess of 10^{11} K/s that are otherwise unattainable.

The effectiveness of such laser-induced heating in shifting branching ratios to processes with high barriers has been shown in earlier studies of the average behavior on surfaces (*6*–*10*). However, its potential for expanding the range of reactions that can be examined with atomic precision by STM had not been recognized. We exploit this capability to determine the microscopic pathway for a model reaction that has attracted great experimental and theoretical interest in the past few years: the recombinative desorption of H_2 from the Si(001) surface (*11*–*15*). Through the measurement reported below, we are able to resolve the discrepancy between the interdimer pathway recently reported for dissociative adsorption of H_2 (*16*) and the intradimer configuration of adsorbed H atoms observed after a conventional thermal desorption process (*17*).

The setup and procedure for the experiment are sketched in Fig. 2. Desorption is induced by focusing the frequency-doubled output of a Nd-YAG (yttrium-aluminum-garnet) laser (wavelength, 532 nm; pulse duration, 7 ns) on the silicon surface in a spot ~500 μm in diameter. The short penetration depth of the radiation leads to heating only within a thin region of the sample near the surface (~1 μm). Thermal diffusion into the bulk material leads to cooling within 10 ns. Because lateral heat flow is negligible, the temperature profile of the surface directly reflects the spatial intensity profile of the laser beam. If only a small fraction of the hydrogen is desorbed from the Si surface, the entire thermally activated process must occur at times when the surface is near its peak temperature. From the known desorption kinetics and modeling heat flow in the substrate, we find that desorption occurs within a time window of just 3 ns. During this short time, we would expect little change in the configuration of the adsorbed hydrogen atoms from diffusion (*18*). It is, however, still necessary to characterize the initial hydrogen distribution on the surface in order to identify the sites that become vacant through the desorption process. For our system, we take advantage of the possibility of preparing nearly perfect monohydride surfaces (i.e., where one atom of hydrogen is adsorbed to every surface silicon atom). In this case, we do not need to image precisely the same region of the surface before and after laser irradiation to infer the desorption pathway, because the initial condition is known everywhere in advance.

The experiments were conducted under ultrahigh vacuum (UHV) conditions at a base pressure of 3×10^{-11} mbar. Silicon surfaces with a combined defect and impurity density below 0.3% were prepared by a method described in (*19*). The monohydride Si(001) sur-

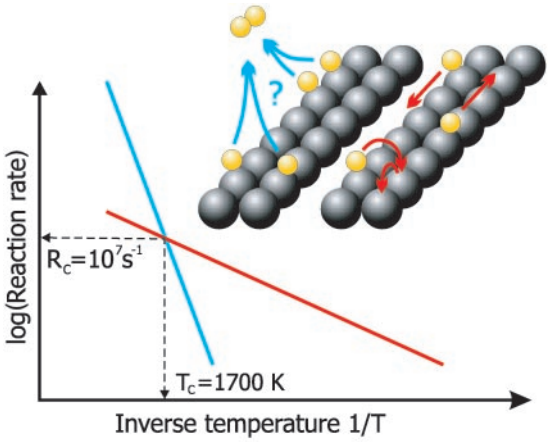

Fig. 1. Illustration of some of the different atomic-scale processes of hydrogen (yellow) possible on the dimer rows of Si(001) (gray). The corresponding temperature dependence is illustrated in a schematic Arrhenius plot where the curves for adatom diffusion (red) and recombinative desorption (blue) cross at a critical temperature T_c with a corresponding rate R_c. For desorption, two pathways have been proposed: an intradimer pathway involving two hydrogen atoms adsorbed on a single Si dimer, and an interdimer pathway involving hydrogen atoms from two adjacent dimers.

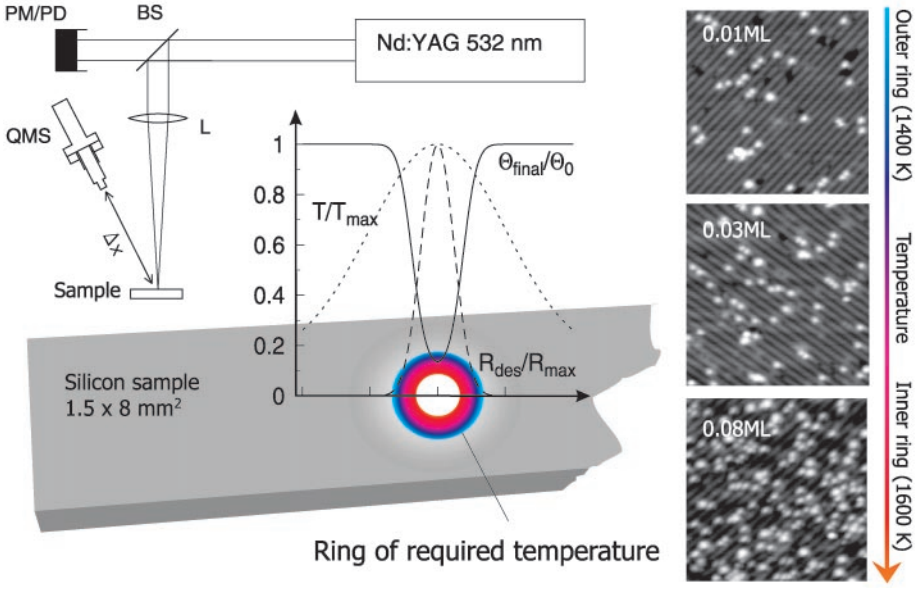

Fig. 2. Experimental setup of the laser-induced desorption measurement. The silicon sample is heated by focusing a nanosecond laser pulse through the lens L. A reference channel is provided by means of a beam splitter (BS) that permits beam characterization with photo diode (PD) and power meter (PM). The temperature rise of the surface leads to recombinative desorption at rate R_{des} from the fully saturated monohydride surface with surface coverage $\Theta_0 = 1$ monolayer (ML). The quadrupole mass spectrometer (QMS) is placed $\Delta x \sim 30$ cm above the sample. The STM images of the resulting surface (right side) exhibit bright features where hydrogen molecules have been desorbed. More desorption (i.e., more bright features) and lower hydrogen coverage Θ_{final} are observed in regions nearer the center of the laser beam where the peak surface temperature is higher. T_{max} and R_{max} denote temperature and desorption rate in the middle of the spot, respectively.

faces were formed by dosing with highly purified hydrogen that was dissociated in situ with a hot tungsten filament. The configuration of adsorbed hydrogen was observed in real space using a commercial room-temperature STM (Omicron STM-1). We explicitly confirmed that only H_2 was desorbed from the surface by the laser heating pulse by means of mass-selected time-of-flight measurements with a quadrupole mass spectrometer.

Figure 3 shows a representative set of STM images under different conditions. On the monohydride surface, the dimer rows as well as the individual silicon dimers are observable. The few unoccupied dangling bonds appear as bright features. The figure also shows the result of desorbing a small fraction of this hydrogen monolayer either by a conventional heating cycle (~650 K for 100 s) or by nanosecond laser heating. In the former case, most of the unoccupied dangling bonds are found paired on the same dimer, in agreement with previous results (*17*). In this configuration, the dangling bonds can form π-like bonds with an effective stabilization energy of ~0.3 eV per dimer. After a nanosecond laser heating cycle, the adsorbate configuration is quite different, as very few of the unsaturated dangling bonds are found in the intradimer configuration of dimer pairs. Rather, one sees a preponderance of pairs of dangling bonds paired on adjacent dimers in the interdimer configuration. To substantiate this observation, we counted the number of each of the four configurations shown in detail in Fig. 3 for a region comprising about 3×10^4 surface atoms. The different configurations are classified by the distance between pairs of dangling bonds along the dimer row; that is, the intradimer configuration has a separation of zero, the interdimer has a separation of one dimer, and so forth (*20*). We made no distinction concerning which side of a dimer was occupied by a dangling bond, because diffusion of hydrogen atoms between these sites is expected to be rapid even for the short duration of the laser heating pulse. Diffusion of hydrogen atoms between adjacent dimer rows is, however, far slower than diffusion along the dimer row (*2, 21*), and no evidence for the occurrence of this process in our experiments has been found.

The site distribution of the unoccupied Si atoms after laser-induced desorption (Fig. 4, middle panel) shows a clear peak for the interdimer configuration. This result is more striking in view of the fact that the intradimer configuration (dangling bond separation = 0) is energetically favored by a few tenths of an eV over the interdimer arrangement. To analyze the data in a more quantitative fashion, we modeled the desorption and subsequent diffusion process for both the inter- and intradimer pathways using the known rate laws (*21, 22*). We find that desorption via an intradimer pathway cannot reproduce the experimental site distribution, even allowing for a range of diffusion times (Fig. 4, lower panel). In such a mechanism, the configuration initially created is the most stable energetically, and there is only a slight population of the other configurations. These arrangements arise simply from the entropy terms in the free energy, which become more important

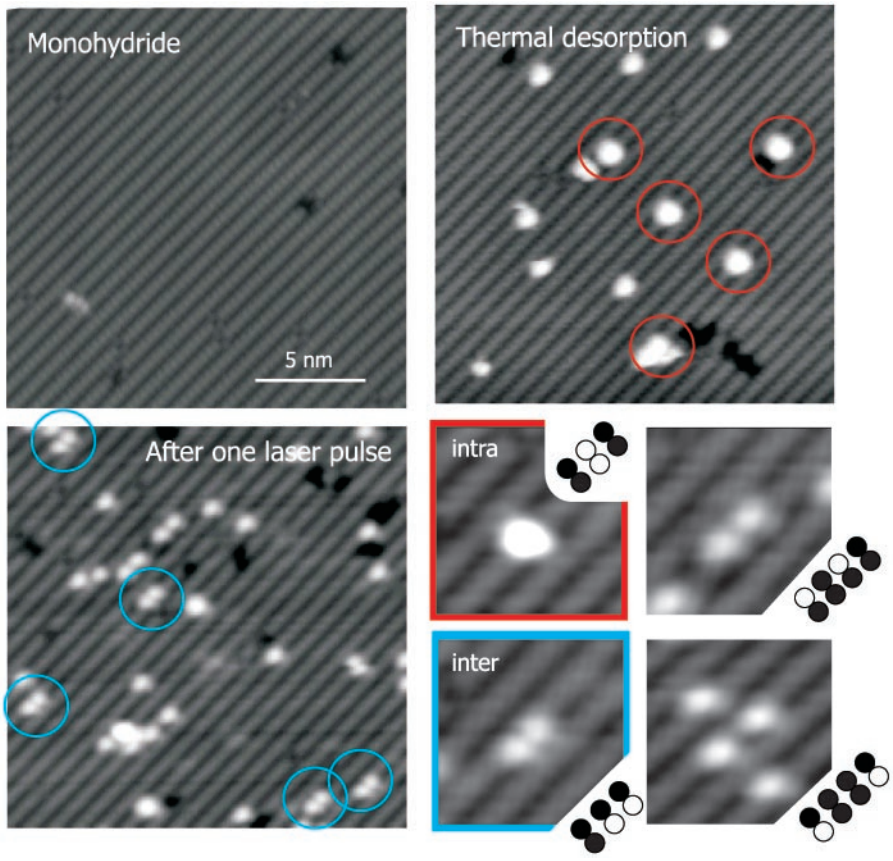

Fig. 3. STM images of the Si(001) surface taken at positive sample voltage $U = +0.8$ V and tunneling current $I = 0.5$ nA. Upper left: The monohydride phase is characterized by the unperturbed dimer row structure of the silicon surface, each small oval comprising two hydrogen-terminated Si surface atoms. Only a few defects (black), unoccupied Si atoms with their dangling bonds (bright), and dihydride sites (symmetrically split dimers) are detectable. After a conventional thermal desorption process (upper right), most of the dangling bonds are paired on the same dimer (marked by red circles). In contrast, after heating by a laser pulse to ~1370 K (lower left), pairs of dangling bonds are found preferentially on adjacent Si dimers (marked by blue circles). The detailed images in the lower right show the different configurations of paired dangling bonds and the corresponding sketches of the structure (a filled circle denotes a hydrogen-terminated Si atom, an unfilled circle denotes a dangling bond): a pair of dangling bonds on the same Si dimer (intra configuration, red label), two dangling bonds on neighboring Si dimers (inter configuration, blue label), as well as two dangling bonds separated by one and by two saturated dimers.

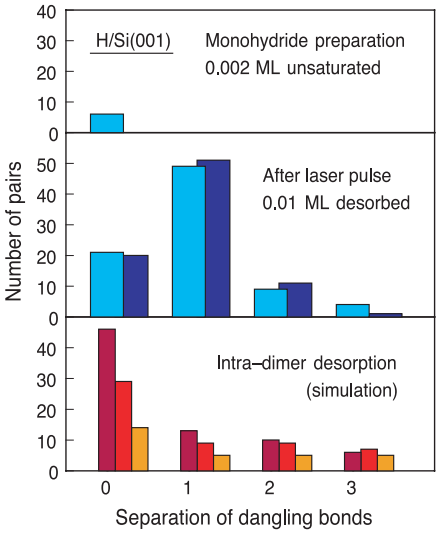

Fig. 4. Measured and simulated distributions of pairs of unsaturated dangling bonds plotted as a function of their separation along the dimer row. Upper panel: Initial condition in the fully saturated monohydride surface. Middle panel: Distribution after nanosecond laser-induced heating, adjusted for the initial condition. The experimental data are shown as light blue bars; the results of a simulation of the desorption process via the interdimer pathway are shown as dark blue bars. Lower panel: Simulation of the desorption process via the intradimer pathway. The different bars correspond to different diffusion times after desorption, from dark red (for diffusion just exceeding the prediction of the rate laws) to orange (for more than an order of magnitude higher diffusion than predicted).

at high surface temperatures. In contrast, a mechanism based on desorption via the interdimer pathway matches the experimental data nicely (Fig. 4, middle panel). The increased population of the intradimer configuration (separation = 0) relative to that for a configuration with a separation of two dimers is attributed to stabilization of the intradimer configuration by the pairing energy described above. We have also analyzed the configurations found in regions of the surface where a greater amount of hydrogen has been desorbed (nearer the center of the laser beam). The results are similar, but experimental observation and model prediction both show a somewhat increased population of the intradimer configuration. This shift arises from the enhanced thermal diffusivity of the adsorbed hydrogen associated with the increased surface temperature.

From the direct imaging of the sites left empty by the laser-induced recombinative desorption of H_2 from the Si(001) surface, we conclude that an interdimer pathway is operative. This finding appears to contradict the observed distribution of hydrogen adatoms after a conventional thermal desorption process (*17*). As discussed above, we understand the discrepancy simply in terms of the rearrangement of the hydrogen atoms by thermal diffusion during the course of the conventional heating cycle. More informative is a comparison of our result for the microscopic pathway for recombinative desorption with the behavior of the time-reversed process of dissociative adsorption of hydrogen. This latter process has been investigated extensively, and recent experiments indicate the existence of an interdimer pathway (*19, 23–26*). Indeed, direct evidence for the interdimer adsorption pathway has been obtained in our laboratory in a real-space STM study (*16*). These experimental results are also consistent with the latest theoretical investigations of the system (*25, 27*).

One might thus be tempted to view the result of the current experiment as an unavoidable consequence of the principle of detailed balance between the reverse processes of adsorption and desorption. This, however, would not be a valid inference. As is generally the case in surface science investigations, the adsorption and desorption measurements were performed under very different conditions. In addition to the fact that neither the adsorption nor the desorption experiments were actually conducted at equilibrium, the experiments probed distinct regimes of hydrogen surface coverage, surface temperature, and kinetic energy of the gas-phase H_2 molecules. Indeed, for this system, a comparison of the kinetic energy dependence of adsorption data taken at low coverage and temperature (*28*) with prior desorption measurements conducted in the high coverage and temperature regime (*29*) yielded certain departures from the predictions of detailed balance. One might then ask—given the complexity of the adsorption-desorption processes and, particularly, the role of displacements of the surface Si atoms—whether the same reaction pathway is followed in these very different regimes. Our experimental results answer this question in the affirmative and demonstrate the robustness of the interdimer adsorption-desorption pathway.

The STM technique illustrated here for the H/Si(001) system permits one to examine elementary reaction steps with substantial barriers that would otherwise be lost for STM analysis because of the presence of diffusion or other low-barrier processes. Potential applications of the method range from probing highly activated diffusion processes (such as ones occurring at steps and affecting crystal growth) to the atomically resolved analysis of product formation in heterogeneous catalysis.

References and Notes

1. J. Wintterlin, S. Völkening, T. V. W. Janssens, T. Zambelli, G. Ertl, *Science* **278**, 1931 (1997).
2. M. McEllistrem, M. Allgeier, J. J. Boland, *Science* **279**, 545 (1998).
3. S. Horch *et al*., *Nature* **398**, 134 (1999).
4. C. Sachs, M. Hildebrand, S. Völkening, J. Wintterlin, G. Ertl, *Science* **293**, 1635 (2001).
5. R. A. van Santen, J. W. Niemantsverdriet, *Chemical Kinetics and Catalysis* (Plenum, New York, 1995).
6. G. Ertl, M. Neumann, *Z. Naturforsch.* **27A**, 1607 (1972).
7. J. P. Cowin, D. J. Auerbach, C. Becker, L. Wharton, *Surf. Sci.* **78**, 545 (1978).
8. R. B. Hall, A. M. DeSantolo, *Surf. Sci.* **137**, 421 (1984).
9. S. M. George, R. B. Hall, A. M. DeSantolo, *Surf. Sci.* **159**, L425 (1985).
10. M. Bonn *et al*., *Science* **285**, 1042 (1999).
11. The earlier investigations have been discussed in several review articles (*12–14*); more recent studies are summarized in (*15, 16*).
12. K. W. Kolasinski, *Int. J. Mod. Phys. B* **21**, 2753 (1995).
13. D. J. Doren, *Adv. Chem. Phys.* **95**, 1 (1996).
14. U. Höfer, *Appl. Phys. A* **63**, 533 (1996).
15. W. Brenig, M. Hilf, *J. Phys. Condens. Matter* **13**, R61 (2001).
16. M. Dürr, Z. Hu, A. Biedermann, U. Höfer, T. F. Heinz, *Phys. Rev. Lett.* **88**, 046104 (2002).
17. J. J. Boland, *Phys. Rev. Lett.* **67**, 1539 (1991).
18. More quantitative analysis yields a peak surface temperature between 1300 and 1500 K, for which the initial desorption sites should be observable by STM for desorption times below 10 ns.
19. A. Biedermann, E. Knoesel, Z. Hu, T. F. Heinz, *Phys. Rev. Lett.* **83**, 1810 (1999).
20. In addition to pairs of unsaturated dangling bonds, some single dangling bonds are seen on the Si(001) surface after laser-induced thermal desorption. We are unable to explain these features by any form of hydrogen adatom diffusion after recombinative desorption, and we attribute these features to a slight uptake of hydrogen atoms into the bulk Si lattice (*30*). This weak process is not expected to influence the recombinative desorption of hydrogen investigated in this study.
21. J. H. G. Owen, D. R. Bowler, C. M. Goringe, K. Miki, G. A. D. Briggs, *Phys. Rev. B* **54**, 14153 (1996).
22. U. Höfer, Leping Li, T. F. Heinz, *Phys. Rev. B* **45**, 9485 (1992).
23. P. Kratzer, E. Pehlke, M. Scheffler, M. B. Raschke, U. Höfer, *Phys. Rev. Lett.* **81**, 5596 (1998).
24. F. M. Zimmermann, X. Pan, *Phys. Rev. Lett.* **85**, 618 (2000).
25. M. Dürr, M. B. Raschke, E. Pehlke, U. Höfer, *Phys. Rev. Lett.* **86**, 123 (2001).
26. M. Dürr, U. Höfer, *Phys. Rev. Lett.* **88**, 076107 (2002).
27. E. Pehlke, *Phys. Rev. B* **62**, 12932 (2000).
28. M. Dürr, M. B. Raschke, U. Höfer, *J. Chem. Phys.* **111**, 10411 (1999).
29. K. W. Kolasinski, W. Nessler, A. D. Meijere, E. Hasselbrink, *Phys. Rev. Lett.* **72**, 1356 (1994).
30. N. M. Johnson, C. Doland, F. Ponce, J. Walker, G. Anderson, *Physica B* **170**, 3 (1991).

31. Supported by the NSF, the Deutsche Forschungsgemeinschaft, the Deutscher Akademischer Austauschdienst (M.D.), and the Alexander von Humboldt Foundation (T.F.H.).

13 February 2002; accepted 29 April 2002

Microfluidic Control Using Colloidal Devices

Alex Terray, John Oakey,* David W. M. Marr*

By manipulating colloidal microspheres within customized channels, we have created micrometer-scale fluid pumps and particulate valves. We describe two positive-displacement designs, a gear and a peristaltic pump, both of which are about the size of a human red blood cell. Two colloidal valve designs are also demonstrated, one actuated and one passive, for the direction of cells or small particles. The use of colloids as both valves and pumps will allow device integration at a density far beyond what is currently achievable by other approaches and may provide a link between fluid manipulation at the macro- and nanoscale.

Microscale devices designed to accomplish specific tasks have repeatedly demonstrated superiority over their macroscale analogs (*1*, *2*). The advantages of such devices are due largely to unique transport properties resulting from laminar flows and vastly increased surface-to-volume ratios (*3*) and have enabled microscale sensors (*4*) and fabrication schemes (*5*) not possible on the macroscale. Additionally, microfluidic processes may be easily parallelized for high throughput (*6*) and require vastly smaller sample volumes, a major benefit for applications in which reagents or analytes are either hazardous or expensive (*7*). The utility, speed,

Chemical Engineering Department, Colorado School of Mines, Golden, CO 80401, USA.

*To whom correspondence should be addressed. E-mail: joakey@mines.edu (J.O.); dmarr@mines.edu (D.W.M.M.)